Available online at www.sciencedirect.com
ScienceDirect
Trans. Nonferrous Met. Soc. China 32(2022) 3110−3122
Transactions of Nonferrous Metals Society of China
www.tnmsc.cn

Enhanced recovery of zinc and lead by slag composition optimization in rotary kiln

Hong-fu LIN[1,2], Wei WENG[2,3], Shui-ping ZHONG[2,3], Guan-zhou QIU[1]

1. School of Minerals Processing and Bioengineering, Central South University, Changsha 410083, China;
2. State Key Laboratory of Comprehensive Utilization of Low Grade Refractory Gold Ores, Zijin Mining Group Co., Ltd., Shanghang 364200, China;
3. Zijin School of Geology and Mining, Fuzhou University, Fuzhou 350108, China

Received 8 November 2021; accepted 25 April 2022

Abstract: High-efficiency recovery of Zn and Pb from silicon-rich zinc leaching residues is realized in a rotary kiln. Characterizations by means of XRD, SEM, EDS and ICP reveal that the leaching residue contains 12.4 wt.% SiO_2, 16.1 wt.% Zn, and 7.4 wt.% Pb. Thermodynamic analysis shows that metallic vapor of Zn and Pb can be easily generated from the zinc leaching residue at 1150−1250 °C inside the rotary kiln. Viscosities and melting points of 13 slag compositions were analyzed and three slag compositions (47wt.%SiO_2−23wt.%CaO−30wt.%FeO, 40wt.%SiO_2−28wt.%CaO−32wt.%FeO, and 40wt.%SiO_2−30wt.%CaO−30wt.%FeO) possessed the desirable physical properties, with the melting point and viscosity in the range of 1150−1280 °C and 0.2−0.5 Pa·s, respectively. The industrial tests show that adopting the optimized slag composition can contribute to very high recovery rates of Zn and Pb (97.3% for Zn and 94.5% for Pb), corresponding to slags with very low average contents of Zn and Pb (0.51 wt.% Zn and 0.45 wt.% Pb). The National-Standard leaching tests of the water-quenched slags result in 1.82 mg/L Zn, ~0.01 mg/L Cu, 0.0004 mg/L As, ~0.01 mg/L Cd, 0.08 mg/L Pb, and ~0.02 mg/L Hg in the leachate, verifying the detoxification of the zinc leaching residue at the same time.

Key words: zinc leaching residues; metals recovery; rotary kiln; slag composition optimization; detoxification

1 Introduction

Worldwide production of zinc in 2020 is more than 1.42×10^7 t, in which 40% of it is produced in China [1]. Generally, production of 1 t metallic zinc results in accumulation of 0.3−0.5 t zinc-leached residues (ZLRs) [1,2], which means that millions of tons of ZLRs are generated annually in China. The ZLRs are valuable secondary resources because of a high zinc content of 6−20 wt.% [3−8]. However, such valuable resources are also solid hazardous wastes posing a long-term threat on the environment due to the entrainment of many other heavy metals such as lead (Pb), cadmium (Cd), and copper (Cu) [9−13]. Therefore, reclamation of these metals within ZLRs can not only contribute to the resource reutilization, but also be beneficial to the detoxification of ZLRs for the harmless disposal [14−16].

Pyrometallurgical recovery of zinc, especially by rotary kiln, is widely adopted for recycling and reutilization of ZLRs [17−21], which possesses two obvious merits: (1) complete detoxification of ZLRs can be achieved; (2) simultaneous recovery of Pb and Zn from ZLRs can be realized, presenting a very simple and short process. Pyrometallurgical reactions of ZLRs in the rotary kiln are highly determined by the physicochemical properties of the SiO_2−CaO−FeO_x slag, which can greatly affect

Corresponding author: Shui-ping ZHONG, Tel: +86-15280385768, E-mail: zspcsu@163.com
DOI: 10.1016/S1003-6326(22)66007-2

the reduction of the oxides and separation of Zn and Pb [17]. Appropriate SiO_2 content is the key for guaranteeing the SiO_2−CaO−FeO_x slag with suitable melting point and viscosity [22,23]. The ZLRs that derive from zinc sulfide concentrates generally possess 4.1−8.5 wt.% SiO_2. However, the SiO_2 content in zinc sulfide concentrates-derived ZLRs is high up to ~12.4 wt.% in southern regions of the Xinjiang Uygur Autonomous Region in China, significantly increasing the difficulties in adjusting the physicochemical properties of SiO_2−CaO−FeO_x slag during the pyrometallurgical process in the rotary kiln. Determining a proper slag composition for guiding the ingredient feeding is critical for the high-efficiency and value-added reutilization of SiO_2-rich ZLRs in southern Xinjiang Uygur Autonomous Region in China.

In this work, based on the properties of the SiO_2-rich ZLRs, optimization strategies of slag composition are proposed for the high-efficiency recovery of Zn and Pb in a rotary kiln. Firstly, to understand the conditions for generation of Zn and Pb metallic vapors in the high-temperature zones, thermodynamic analyses for ZLRs-reduction-involved chemical reactions are conducted. Then, melting points and viscosities of thirteen slag compositions are compared and proper slag compositions for pyrometallurgy in the rotary kiln are suggested. Finally, industrial tests are performed based on the suggested slag compositions to verify the high-efficiency recovery of Zn and Pb in the SiO_2-rich ZLRs. The results will provide new insights for guiding the ingredient feeding to realize the industrially high-efficiency reutilization and detoxification of SiO_2-rich ZLRs.

2 Experimental

2.1 Materials characterization

The ZLRs samples taken from Xinjiang Zijin Nonferrous Metals Co., Ltd., in southern Xinjiang Uygur Autonomous Region in China were dried at 60 °C for more than 24 h before use, and then analyzed by inductively coupled plasma atomic emission spectrometry (ICP-AES, AMETEK, SPECTROBLUE, FMS36) to determine the chemical composition. The typical composition of the ZLRs used in this work is shown in Table 1. The composition of ZLRs-derived slag was also analyzed by the similar way. The content of metallic iron in the slag was determined by a strong magnet. The metallic iron was excluded during the SiO_2−CaO−FeO ternary slag composition analysis. The phase structures of all solid samples were detected by X-ray diffraction spectroscopy (XRD, Shimadzu X-ray 6000 with Cu $K_{\alpha 1}$ radiation at λ=1.5405 Å). The morphologies of ZLRs and ZLRs-derived slags were analyzed by a thermal field emission scanning electron microscope (SEM) coupled with an energy-dispersive X-ray spectrometer (EDS, JMS−7610F, Japan).

Table 1 Typical composition of SiO_2-rich ZLRs used in this work (wt.%)

Zn	SiO_2	Pb	CaO	S	Fe	Al_2O_3
16.1	12.4	7.4	2.5	9.6	18	2.3

2.2 Viscosity determination

The SiO_2, CaO, Fe powder and Fe_2O_3 were of analytical purity and provided by Aladdin (Shanghai, China). FeO in the molten slag was generated by reaction between Fe_2O_3 and Fe powder [22,23]. Specifically, the mixture of 1 mol Fe powder and 1 mol Fe_2O_3 resulted in 3 mol FeO. The Fe−Fe_2O_3 mixture was well mixed with the pre-determined amounts of SiO_2 and CaO. The SiO_2−CaO−Fe_2O_3−Fe powders were then melted in a tube furnace at 1400 °C protected by a high-purity argon gas flow of 100 mL/min. It should be noted that, extra 10 wt.% Fe powder was added to enable the stable existence of FeO in the molten slags. Finally, the viscosities of the melted slags were determined by the rotating technique using Brookfield DVIII+ rheometer, Mo spindle, and crucible. Generally, ~100 g molten slag was used for all tests and high-purity argon gas (100 mL/min) was purged to provide an inert atmosphere.

2.3 Industrial tests

The industrial tests were conducted in a rotary kiln, with the inner diameter and length of 4.15 m and 58 m, respectively. Generally, the ZLRs, coke powder, and calcine oxide were well mixed. The mixture was continuously fed into the rotary kiln from the end side, with the compressed air being concurrently blown into the kiln from the other side. The mass ratio of coke powder to ZLRs was fixed as 0.5:1, and the feeding amount of the mixture was 21 t/h, namely 504 t/d. The calcine oxide was added based on the predetermined mass

ratio of SiO_2 to CaO. The gas flow of compressed air was 9000 m^3/h, and the air pressure was 0.14−0.16 MPa. The inclination and revolving speed of the rotary kiln were 5° and 0.5 r/min, respectively. The mixtures inside the rotary kiln slid from the end side to the head side of the kiln, which lasted for about 2 h and were converted to SiO_2−CaO−FeO slags, were discharged into a water quenching pool for sale. The toxic leaching experiments were conducted according to the Chinese National Standard (GB 5086.2—1997).

3 Results and discussion

3.1 SiO_2-rich characteristics of ZLRs and slags

The SiO_2 content of ZLRs in Xinjiang Zijin Nonferrous Metals Co., Ltd., China (Labeled as This work or ZLR-0 in Fig. 1) is much higher than that of other zinc plants. The SiO_2 content of zinc sulfide concentrates-derived ZLRs is commonly located in the range of 4.1−8.5 wt.% [1−6]. However, the value of ZLRs used in this work is high up to 12.4 wt.% (Table 2). The stronger diffraction intensity of SiO_2 in the XRD pattern of ZLR-0 (This work) than that of ZLR-1 (ZLR-1 in Table 2) also reveals a higher SiO_2 content in the former case (Figs. 1(a) and (b)). In addition to SiO_2 (JCPDS No. 87-2096), $ZnFe_2O_4$ (JCPDS No. 79-1150), $PbSO_4$ (JCPDS No. 05-0577), and ZnS (JCPDS No. 65-9585) are also obviously detected in the XRD patterns of both ZLR-0 and ZLR-1 [1−6], showing that both samples possess similar zinc-containing phases. The higher SiO_2 content in ZLR-0 is also implied by more agglomerated particles than that of ZLR-1 (Figs. 2(a) and (b)) due to the existence of more silica gel in the former case [9]. Such results are further manifested by the higher peak intensity of Si in the EDS spectrum of ZLR-0 than that of ZLR-1 (Fig. 2(c)), which is validated by the EDS composition results (11 wt.% Si for ZLR-0 vs 5 wt.% Si for ZLR-1, see Table 3). The above results all point to a much higher SiO_2 content of ZLR-0 (sample in this work) than the industrial average value. Such a high SiO_2 content in ZLRs means that the SiO_2−CaO−FeO slag composition should be deliberately tuned to maximize the recovery of Zn and Pb during the pyrometallurgical reduction−volatilization process of ZLRs in the rotary kiln.

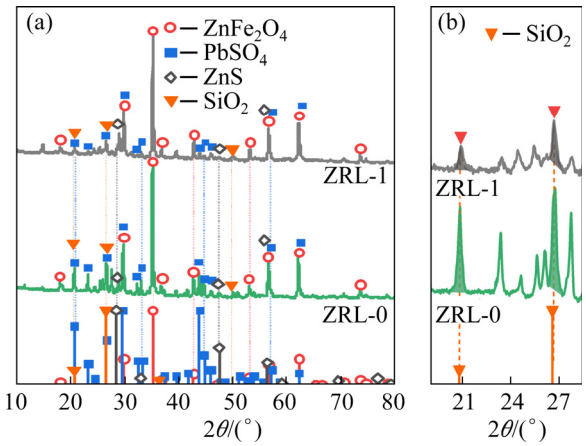

Fig. 1 XRD patterns of ZLRs: (a) 2θ of 10°−80°; (b) 2θ of 20°−28°

Table 2 SiO_2 content of seven different ZLRs in China (wt.%)

ZLR-1	ZLR-2	ZLR-3	ZLR-4	ZLR-5	ZLR-6	This work
4.1	5	7	7.6	8.3	8.5	12.4

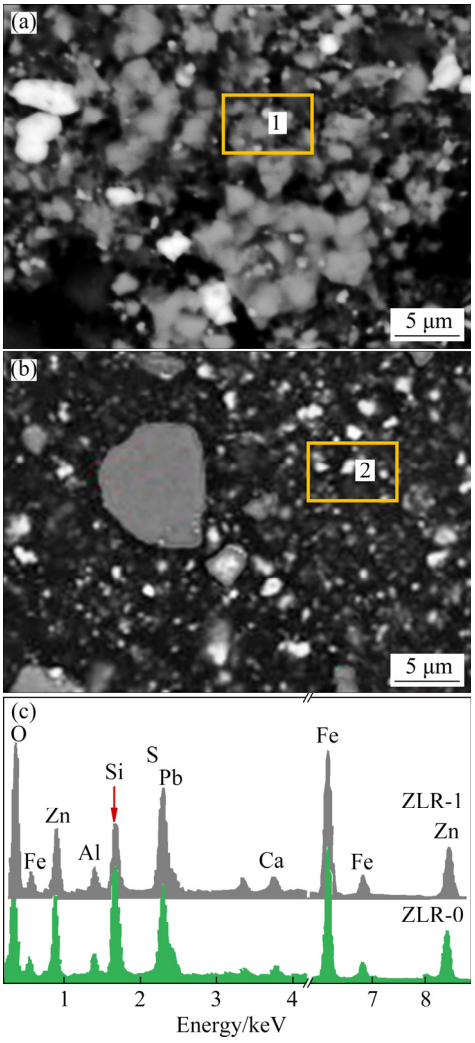

Fig. 2 SEM images of ZLR-0 (a) and ZLR-1 (b), and EDS results of Areas 1 and 2 (c)

Table 3 Corresponding compositions for EDS results in Fig. 2(c) (wt.%)

Sample	Zn	Pb	Si	S	Fe	Ca	Al	O
ZLR-0	21	10	11	7	25	1	2	23
ZLR-1	18	7	5	9	31	2	3	25

Compared with ZLR-1, the high SiO_2 content in the ZLR-0 results in much higher contents of SiO_2-containing phases in the rotary kiln slag, leading to different SiO_2−CaO−FeO ternary slag compositions between RKS-0 and RKS-1. As shown in Fig. 3, both RKS-0 and RKS-1 consist of SiO_2 (JCPDS No. 87-2096), FeS (JCPDS No. 24-0080), $CaFeSi_2O_6$ (JCPDS No. 87-1699), $FeSiO_4$ (JCPDS No. 87-0320) and $CaFe_2O_4$ (JCPDS No. 03-0825), but with stronger peak intensities of SiO_2 and SiO_2-containing phases for the former case. The similar phase components between RKS-0 and RKS-1 are also revealed by the almost same morphologies (Fig. 4). The results imply that RKS-0 and RKS-1 present similar phase components, but possessing higher contents of SiO_2-related phases in RKS-0. Therefore, huge difference exists in the SiO_2−CaO−FeO ternary-phase slag composition between RKS-0 and RKS-1. Such results are further manifested by the much higher peak intensity of Si for RKS-0 than RKS-1

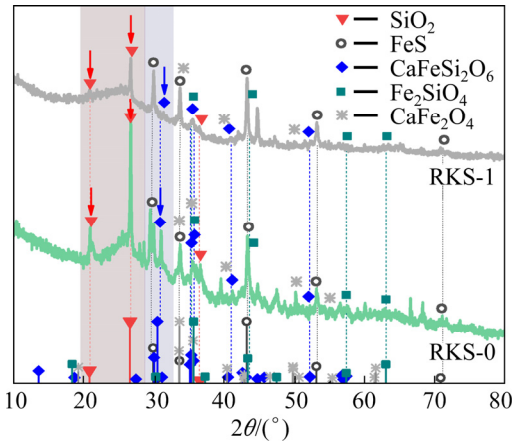

Fig. 3 XRD patterns of rotary kiln slags (RKS-0: Rotary kiln slag derived from ZLR-0; RKS-1: Rotary kiln slag derived from ZLR-1)

in EDS results (Fig. 5). More specifically, the EDS results show 31 wt.% Si for RKS-0, much higher than that (14 wt.%) of RKS-1, again implying the huge difference in slag composition between the two samples (Table 4). The EDS results also show that the RKS-0 possesses higher Al content than RKS-1, which is attributed to the falling off of the high-alumina-content furnace lining, showing that the SiO_2-rich property aggravates the chemical corrosion of the furnace lining.

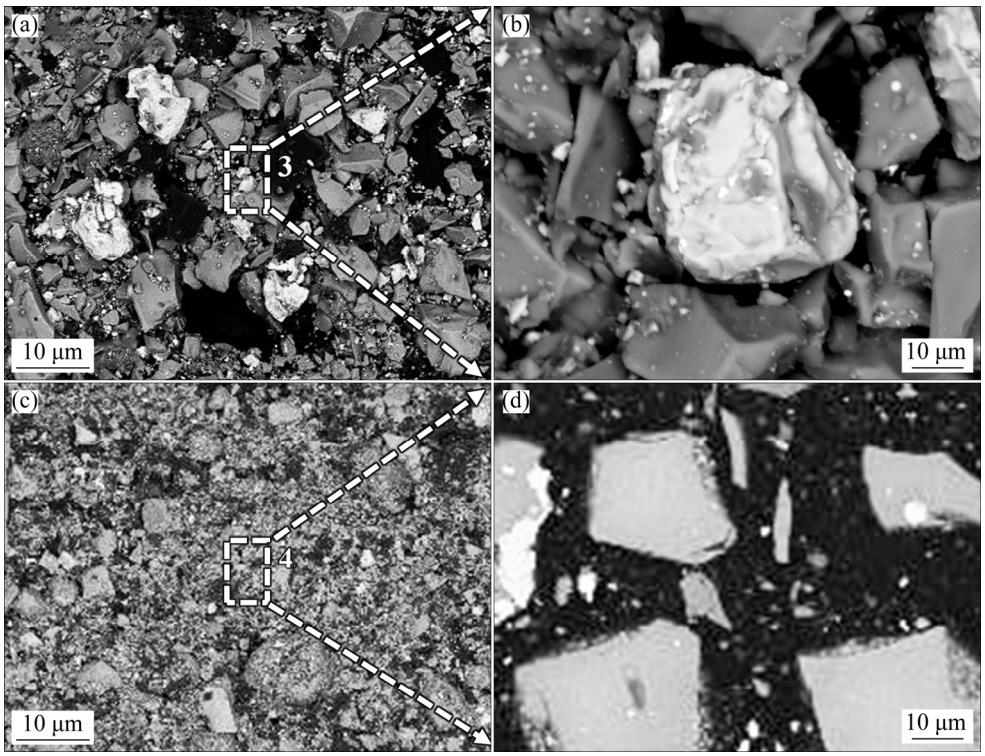

Fig. 4 SEM images of rotary kiln slags: (a, b) RKS-0; (c, d) RKS-1

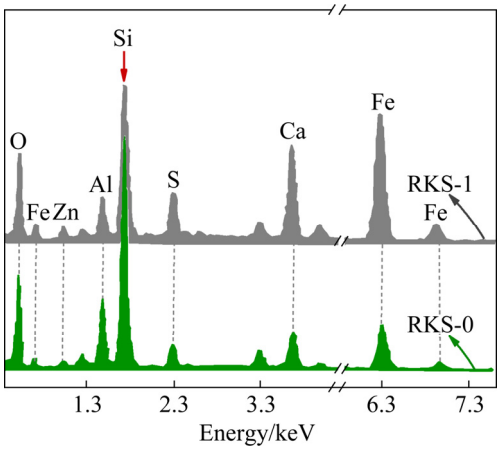

Fig. 5 EDS results of rotary kiln slags (RKS-0 is taken from Area 3 in Fig. 4(a), and RKS-1 is taken from Area 4 in Fig. 4(c))

Table 4 Corresponding compositions for EDS results in Fig. 5 (wt.%)

Sample	Si	Fe	Ca	S	O	Zn
RKS-0	21	10	11	7	25	1
RKS-1	18	7	5	9	31	2

The ZLRs in this wok possess a much higher SiO_2 content, resulting in much higher contents of SiO_2-related phases in the ZLRs-derived slags after pyrometallurgical recovery of Zn and Pb in the rotary kiln. The huge composition difference in the slag-forming elements of Si, Fe, Ca and O implies totally different physicochemical properties of SiO_2−CaO−FeO slags, probably resulting in great discrepancy in recovery of Zn and Pb.

3.2 Chemical reactions inside kiln and physicochemical properties of slag

High-efficiency pyrometallurgical recovery of Zn and Pb by rotary kiln is highly determined by two factors: the chemical reactions inside the rotary kiln and physicochemical properties of the SiO_2−CaO−FeO slag. The chemical reactions involving the reduction of Zn-containing and Pb-containing phases determine the efficient conversion of ZnO and PbO to gaseous Zn and Pb. The physicochemical properties of SiO_2−CaO−FeO slag can greatly affect the separation of gaseous Zn and Pb from the slags. Therefore, understanding the chemical reactions for the reductions of Zn/Pb-containing phases inside the rotary kiln and properly tuning the physicochemical properties of the SiO_2−CaO−FeO slag are essential for enhancing the pyrometallurgical recovery of Zn and Pb in the rotary kiln.

$ZnFe_2O_4$ and $PbSO_4$ are the main Zn-containing and Pb-containing phases in the zinc-leached residues (Fig. 1) and their reduction routes are understood based on the thermodynamics analysis (Figs. 6 and 7). During the pyrometallurgical reduction−volatilization recovery of Zn and Pb from the zinc-leached residues in the rotary kiln, both C and CO act as the reducing agents. Figure 6 presents the Gibbs free energy changes (ΔG) for the reduction reactions of $ZnFe_2O_4$, revealing that ZnO and FeO are the main reduction products. CO can only reduce $ZnFe_2O_4$ to ZnO (Red line in Fig. 6(a), negative values of ΔG) rather than gaseous Zn (Grey line in Fig. 6(a), positive values of ΔG). Similarly, for the reduction of $ZnFe_2O_4$ by C, formation of ZnO is easier than that of metallic Zn (Red line vs Grey line in Fig. 6(b)), as manifested by the much smaller ΔG values for the former case. Therefore, $ZnFe_2O_4$ is preferentially reduced to ZnO and FeO in the rotary kiln. Subsequently, the generated ZnO is further reduced to gaseous metallic Zn by CO (Fig. 6(c)) or C (Fig. 6(d)). Notably, generation of gaseous Zn from the reduction of $ZnFe_2O_4$-derived ZnO by CO, namely $ZnO+CO(g)=Zn(g)+CO_2(g)$, can be greatly promoted in the high-temperature reaction zone (950−1250 °C) due to the following merits: (1) low CO_2 partial pressure. When C exists, CO_2 can be converted to CO at high temperatures ($CO_2+C=2CO$, $\Delta G<0$ at temperatures exceeding 700 °C); (2) Low partial pressure of gaseous Zn. During the pyrometallurgical reduction−volatilization recovery of Zn and Pb from the zinc-leached residues in the rotary kiln, a huge amount of compressed air (9000 m^3/h) is blown into the kiln. Therefore, N_2 and CO are the main components in the gas atmosphere, meaning that the partial pressure of gaseous Zn is much lower than 1. In addition, oxidation of gaseous Zn by the remaining O_2 in the gas atmosphere can take place very easily, further decreasing the partial pressure of gaseous Zn. The above factors can enhance the reduction of ZnO by CO, as implied by the significantly decreased values of ΔG (Fig. 6(c)) when reducing the p_{CO_2}/p_{CO} (from 1 to 0.1) and $p_{Zn(g)}$ (from 1 to 0.2). Compared with $ZnFe_2O_4$, reduction of $PbSO_4$ undergoes a very different route, which means that

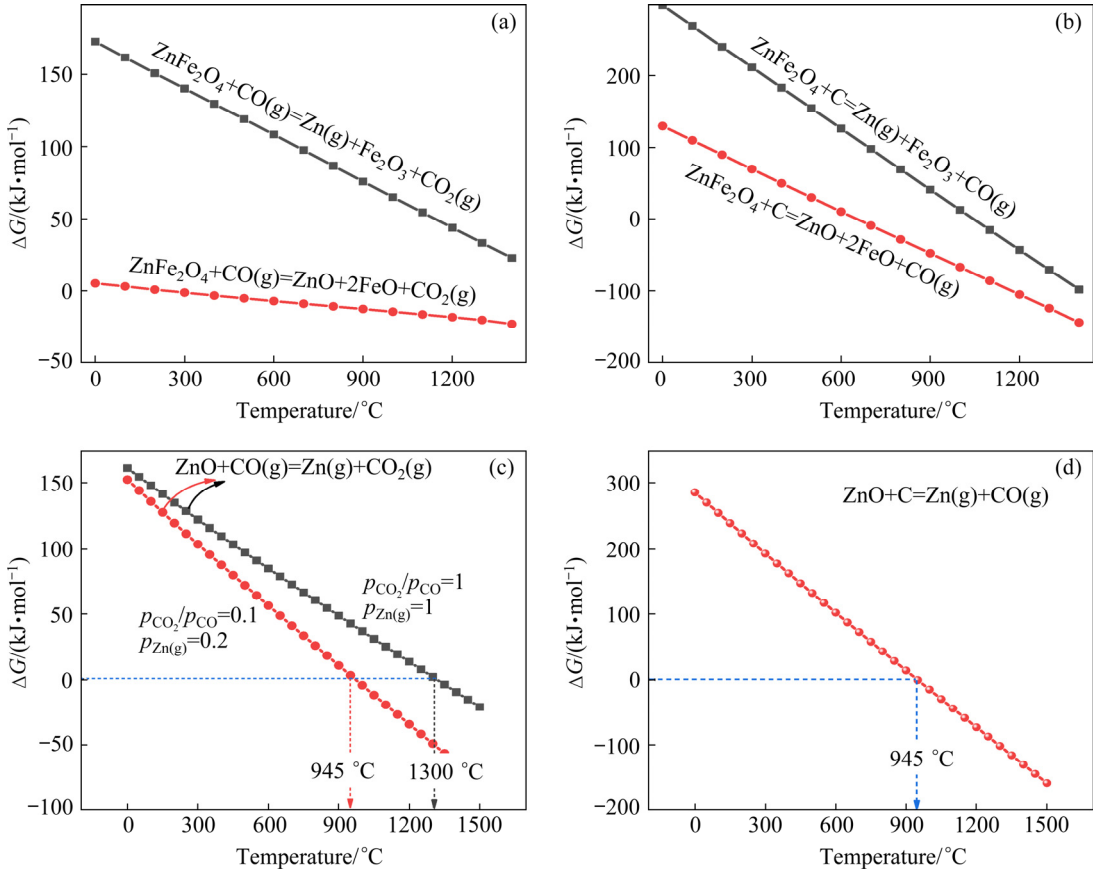

Fig. 6 Gibbs free energy changes vs temperature for possible reactions: (a) Reduction of $ZnFe_2O_4$ by CO; (b) Reduction of $ZnFe_2O_4$ by C; (c) Reduction of ZnO by CO; (d) Reduction of ZnO by C (The HSC 6.0 software was used for calculating the Gibbs free energy changes. p_{CO_2} denotes the ratio between the partial pressure of CO_2 and the standard atmosphere pressure. $p_{Zn(g)}$ denotes the ratio between the partial pressure of gaseous Zn and the standard atmosphere pressure. p_{CO} denotes the ratio between the partial pressure of CO and the standard atmosphere pressure.)

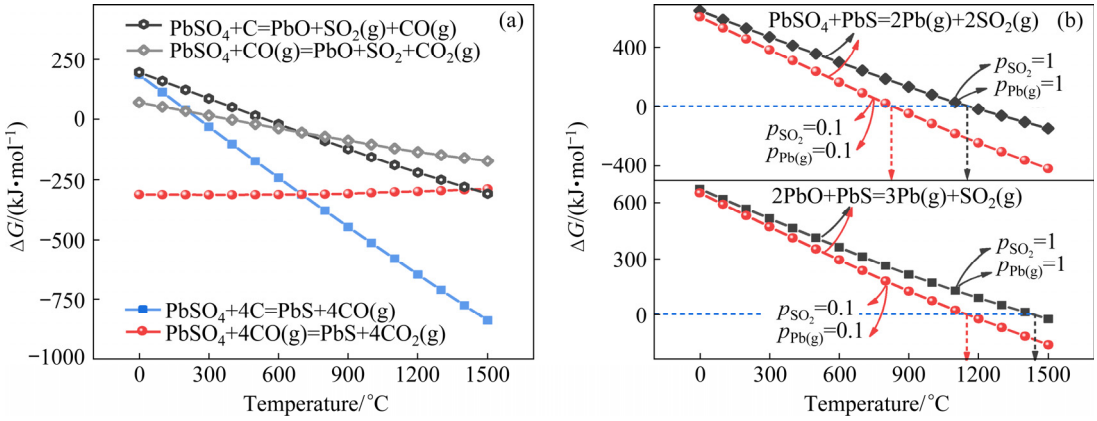

Fig. 7 Gibbs free energy changes vs temperature for possible reactions: (a) Reduction of $PbSO_4$ by C or CO; (b) Reaction between $PbSO_4$, PbS, and PbO (The HSC 6.0 software was used for calculating the Gibbs free energy changes. p_{SO_2} denotes the ratio between the partial pressure of SO_2 and the standard atmosphere pressure. $p_{Pb(g)}$ denotes the ratio between the partial pressure of gaseous Pb and the standard atmosphere pressure.)

$PbSO_4$ is firstly reduced to PbS (Fig. 7(a)) and then further converted to gaseous Pb (Fig. 7(b)). For the reduction of $PbSO_4$ by both C and CO (Fig. 7(a)), formation of PbS (Red and blue lines in Fig. 7(a)) is easier than that of PbO (Black and grey lines in Fig. 7(a)), as validated by the much more negative values of ΔG for the former cases. The generated PbS can be further converted to gaseous metallic Pb

and SO_2 by reaction with the remaining $PbSO_4$ or generated PbO. Notably, the low partial pressures of both SO_2 (~0.8 vol.%) and gaseous Pb can promote the reactions in Fig. 7(b), as manifested by the obviously decreased ΔG values when the partial pressures of SO_2 (p_{SO_2}) and Pb ($p_{Pb(g)}$) decrease from 1 to 0.1 (Fig. 7(b)).

In addition to the chemical reactions, the physicochemical property of the SiO_2−CaO−FeO slag can also affect the pyrometallurgical recovery of Zn and Pb from ZLRs in the rotary kiln. The melting point is the first important physicochemical property of the SiO_2−CaO−FeO slag, which can determine the existing states of the slag and influence the kinetics of both reactions and volatilization process. The temperature of reaction zones inside the rotary kiln locates in the range of 1150−1250 °C. As shown in Fig. 8(a), the SiO_2−CaO−FeO slag in the light orange region (Fig. 8(a)) possesses much lower melting points (1100−1150 °C, denoted as Area 4 in Fig. 8(b)) than the rotary kiln reaction zone temperature (1150−1250 °C), therefore being well melted inside the rotary kiln. On the contrary, the light blue region in Fig. 8(a) denotes the SiO_2−CaO−FeO slag with the melting point range of 1400−1600 °C (marked as Area 1 in Fig. 8(b)), which is much higher than the rotary kiln reaction zone temperature (1150−1250 °C), therefore being not melted inside the rotary kiln. Correspondingly, the yellow, red, and green regions (Areas 2, 3 and 5 in Fig. 8(b)) possess a melting point of 1150−1400 °C, which is close to the rotary kiln reaction zone temperature (1150−1250 °C), therefore mainly existing as half-melted state in the reaction zone during pyrometallurgical process. Conclusively, the SiO_2−CaO−FeO slags with the compositions located in Areas 2, 3 and 5 result in half-melted slag in the reaction zone of the rotary kiln, while the SiO_2−CaO−FeO compositions in Areas 1 and 4 lead to unmelted and fully melted slags, respectively.

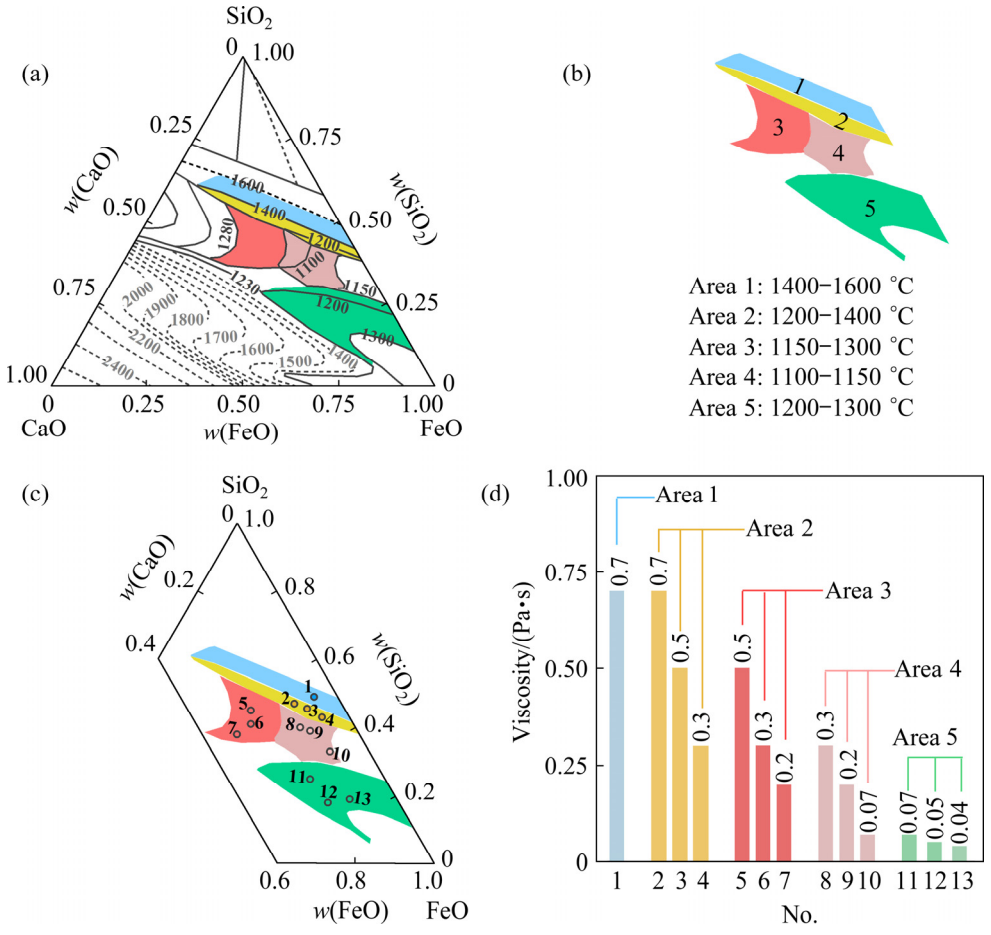

Fig. 8 SiO_2−CaO−FeO ternary isothermal phase diagram (a), region division based on melting points in SiO_2−CaO−FeO ternary phase diagram (b), experimental compositions of points labeled as 1−13 (c), and viscosity of tested compositions at 1400 °C (d)

The viscosity is another physicochemical property of the SiO_2−CaO−FeO slag that can affect the pyrometallurgical process. Too viscous slag can aggravate the ring formation inside the rotary kiln [19,20,24,25], which can stumble the volatilization of ZnO and PbO dusts. The viscosities of 13 composition points are tested, with their specific located areas in the SiO_2−CaO−FeO ternary phase diagram detailed in Fig. 8(c). It should be mentioned that all viscosity tests were conducted at 1400 °C to enable the full melting of the slags. As shown in Fig. 8(d), the viscosity of SiO_2−CaO−FeO slag roughly decreases progressively from Area 1 to Area 5, which obeys the similar trend with the reported values in the literature [23,26,27], validating the high reliability for the viscosity tests in this work. The results indicate that increasing the SiO_2 content results in more viscous slag while adding FeO or CaO contributes to less viscous slag in the investigated areas.

In conclusion, the reduction reactions of both $ZnFe_2O_4$ and $PbSO_4$ as well as the physicochemical properties of the SiO_2−CaO−FeO slag are well analyzed. The $ZnFe_2O_4$ and $PbSO_4$ undergo totally different conversion routes during the pyrometallurgical reduction−volatilization process. The physicochemical properties of the SiO_2−CaO−FeO slag, including both the melting point and viscosity, are highly dependent on the compositions. Therefore, tuning the SiO_2−CaO−FeO slag composition can greatly adjust the reaction kinetics, being an effective way for enhancing the pyrometallurgical reduction−volatilization process.

3.3 Industrial validations

Industrial tests show that keeping the slag compositions in Areas 2, 3, and 5 in the SiO_2−CaO−FeO ternary phase diagram can enable the high-efficiency recovery of Zn and Pb. The industrial tests were conducted in a rotary kiln, with the inner diameter and length of 4.15 and 58 m respectively. The mixtures (21 t/h) of ZLR-0, coke powder, and calcine oxide are continuously fed into the rotary kiln, with the added amount of calcine oxide being deliberately tuned to adjust the slag compositions. The tested slag compositions are controlled to locate at different areas in the SiO_2−CaO−FeO ternary isothermal phase diagram, being marked as A, B, C, D, E, F, G, H, I, and J in Fig. 9(a). After pyrometallurgical process, the SiO_2−CaO−FeO slags located at Areas 2, 3, and 5 contain much less entrained Zn content (0.16−1.2 wt.%, see Fig. 9(b)) than those in both Area 1 (2.8−2.9 wt.% Zn, see Fig. 9(b)) and Area 4 (1.98−2.5 wt.% Zn, see Fig. 9(b)). The OM images of both the hot (Fig. 10(a)) and solidified (Fig. 10(b)) slags in Area 3 show a highly porous characteristic, with a honeycomb-like structure being clearly uncovered (Fig. 10(b)). Such a porous property can contribute to superior reaction kinetics for the reduction of ZnO and PbO, namely more reactive surface area between coke powders and the ZnO/PbO-containing phases as well as easier penetration of CO into the porous slags, therefore resulting in the high-efficiency recovery of Zn and Pb from the slags. The superiority of the honeycomb-like slag is further manifested by repeated industrial tests for half a month, with the

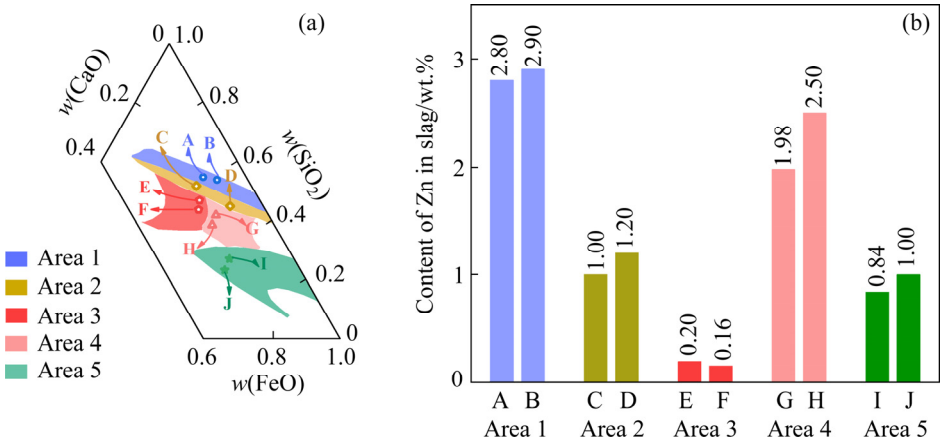

Fig. 9 Ten industrially tested SiO_2−CaO−FeO slag compositions for pyrometallurgical recovery of Zn and Pb from SiO_2-rich ZLRs (ZLR-0 in Fig. 1) (a), and remaining Zn contents in SiO_2-rich ZLRs-derived slags after industrial testing (b)

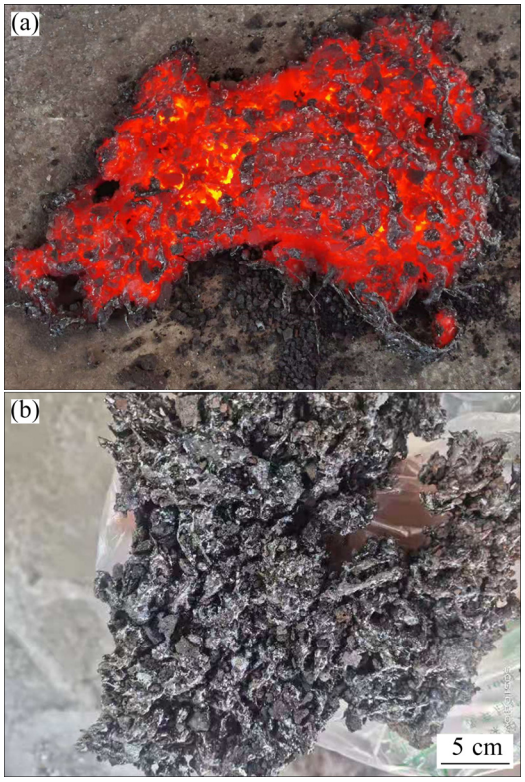

Fig. 10 Optical photos of slags from E in Fig. 9: (a) Hot state; (b) Solidified state

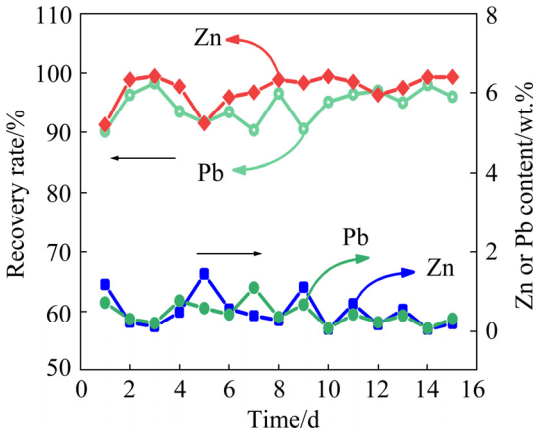

Fig. 11 Recovery rates of Zn and Pb from SiO_2-rich ZLRs (ZLR-0 in Fig. 1) as well as Zn and Pb contents in SiO_2−CaO−FeO slags (The SiO_2−CaO−FeO slag compositions for all tests are fixed as E)

Table 5 Typical slag composition for Fig. 11 (wt.%)

Zn	Pb	SiO_2	Fe	CaO	Fe^0	S	Al_2O_3
0.5	0.4	28	27.5	10	11.1	5.5	5.1

Fe^0: Metallic iron

slag composition being fixed as E (see Fig. 11). As shown in Fig. 11, the repeated industrial tests result in a stable recovery rate of 91%–98% for both Zn and Pb, corresponding to a very low average Zn content of 0.51 wt.% and average Pb content of 0.45 wt.% in the slag. The typical slag composition for Fig. 11 is shown in Table 5. The above industrial tests again manifest that high recovery of Zn and Pb can be realized by adopting suitable slag compositions during the pyrometallurgical process of ZLRs in the rotary kiln.

To further understand the effect of slag compositions on the recovery rate of Zn and Pb, the OM images of slags in different areas are compared (Fig. 12). In Fig. 12(a), the presented slag is in Area 1, with the composition of 54wt.%SiO_2−9wt.%CaO−37wt.%FeO, corresponding to a melting point (T_m) of about 1500 °C. Obviously, the melting point of the slag is much higher than the reaction zone temperature (1150−1250 °C) in the rotary kiln, which means that the slag exists as solid state (Fig. 12(a)) during the pyrometallurgical process, leading to a very high entrained Zn content in the rotary kiln slag (2.9 wt.%, Fig. 12(a)). In Fig. 12(b), the presented slag is in Area 3, with the composition of 47wt.%SiO_2−16wt.%CaO−37wt.%FeO, corresponding to a melting point of about 1170 °C. Such a melting point is very close to the reaction zone temperature (1150−1250 °C) in the rotary kiln, which implies that the slag in this area is softened, but with poor fluidity at the same time (Fig. 12(b)). The softened slag can improve the reaction kinetics while the poor fluidity can keep the highly porous structure, therefore contributing to a very low entrained Zn content in the rotary kiln slag (0.2 wt.%, Fig. 12(b)). In Fig. 12(c), the presented slag is in Area 4, showing a high fluidity (Fig. 12(c)) due to a very low melting point of 1100 °C (38wt.%SiO_2−15wt.%CaO−47wt.%FeO). The improved fluidity means poor porosity, which can impede both the metal vapor volatilization and CO penetration, resulting in increased Zn entrainment in the slag when compared with that in Fig. 12(b) (1.1 wt.% Zn vs 0.2 wt.% Zn).

The existing states for the mixture of zinc-leached residue and coke powder in the rotary kiln are illustrated in Fig. 13. For the slags in Area 1 that are not melted (Fig. 13), reaction between zinc-leached residues and coke powders is difficult to proceed smoothly due to the point-to-point contact state, which means limited reaction areas.

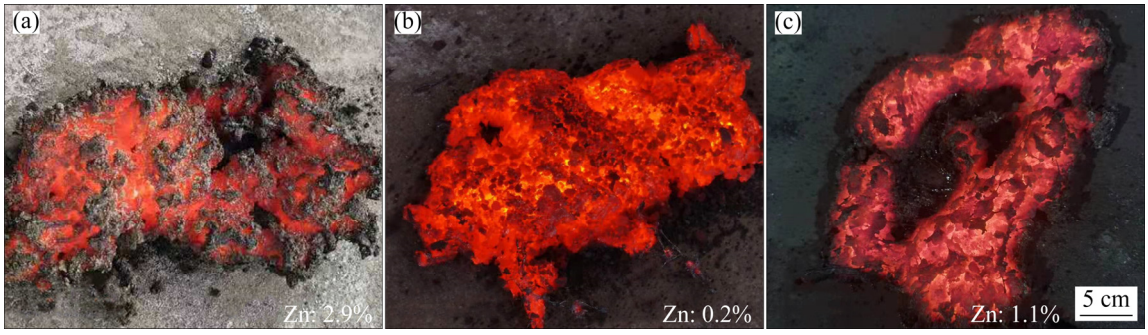

Fig. 12 Optical photos of slags derived from ZLR-0 during pyrometallurgical recovery of Zn and Pb in industrial production: (a) Area 1, slag composition of 54wt.%SiO_2−9wt.%CaO−37wt.%FeO, and T_m of 1500 °C; (b) Area 3, slag composition of 47wt.%SiO_2−16wt.%CaO−37wt.%FeO, and T_m of 1170 °C; (c) Area 4, slag composition of 38wt.%SiO_2−15wt.%CaO−47wt.%FeO, and T_m of 1100 °C

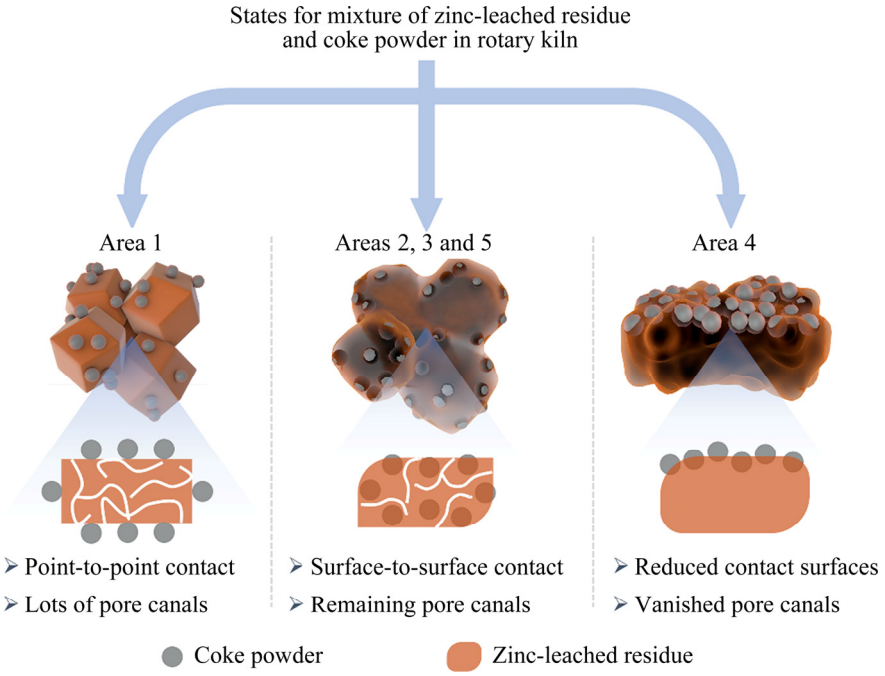

Fig. 13 Illustration for physicochemical characteristics between coke and slags with different states

The unmelted slags also lead to the difficulties for the deep reduction of ZnO-containing phases by CO because these phases are locked inside the solid slags and hard to contact with CO [28,29]. Compared with unmelted slags, the slags in Areas 2, 3, and 5 are softened, which can result in the partial embedment of coke powder inside the slags and turn the point-to-point contact state to surface-to-surface contact condition (Fig. 13), contributing to more reactive surface areas. In addition, the softened slags can result in oscillation-induced movement of the ZnO-containing phases to the outer surfaces of the slags, contributing to smoother reduction of ZnO by CO in the gas atmosphere. Moreover, the low-fluidity of the slags in these areas can maintain the porous structure (Fig. 13), facilitating the permeation of CO for deeper reduction reactions. However, pore canals in the fully melted slags with high fluidity (Area 4, Fig. 13) will disappear completely, avoiding the penetration of CO into the slags. What's worse, the fully melted slags can lead to the floating of coke powders on the upper surface of liquidous slags, leading to largely decreased reactive contact areas. Moreover, the low melting point slag can increase the erosion of kiln lining and at the same time make the burden sticky, forming rings after repeated rolling. In conclusion, the SiO_2−CaO−FeO slags in Areas 2, 3, and 5 with desirable physicochemical properties contribute to optimum reaction kinetics, enabling a deeper pyrometallurgical recovery of Zn and Pb in the rotary kiln.

The detoxification of the ZLRs can be also realized. The leaching tests of the water-quenched slags are conducted according to the experimental requirements of National Standard (GB 5086.2—1997). The concentrations of typical heavy metals in the leachate are presented in Table 6, which clearly shows that the experimental values are all much lower than the limiting values in the National Standard (GB 5086.2 — 1997), meaning the nontoxic properties of the slags. Therefore, the complete detoxification of the hazardous ZLRs is realized after pyrometallurgical process in the rotary kiln.

Table 6 Limiting values in National Standard (GB 5086.2 — 1997) and experimental values for concentration of typical heavy metals in leachate (mg/L)

Element	Standard limiting value	Experimental value
Zn	100	1.85
Cu	100	<0.01
As	5	0.0004
Cd	1	<0.01
Pb	5	0.08
Hg	0.1	<0.02
Ni	5	0.1
Cr	15	<0.01
Ba	100	0.079

In a word, the high-efficiency recovery of Zn and Pb as well as deep detoxification can be realized by the pyrometallurgical reduction−volatilization process of hazardous ZLRs in the rotary kiln. Specifically, the suitable slag composition areas, namely the Areas 2, 3, and 5, are determined in the SiO_2−CaO−FeO ternary isothermal phase diagram. For the SiO_2-rich ZLRs, the Areas 2 and 3 are the preferable slag compositions due to the characteristics of high-SiO_2 and low-FeO contents in these areas. After the pyrometallurgical process, the hazardous ZLRs-derived slags are completely converted to nontoxic slags.

4 Conclusions

(1) The SiO_2-rich property of the ZLRs is verified. The SiO_2 content in the ZLRs is high up to 12.4 wt.%, which is much higher than that (4.1−8.5 wt.%) of commonly used zinc sulfide concentrates-derived ZLRs.

(2) The proper slag compositions for the high-efficiency recovery of Zn and Pb from SiO_2-rich ZLRs in the rotary kiln are suggested. Five slag composition regions in the FeO−SiO_2−CaO ternary phase diagram are analyzed based on the melting point and viscosity. The regions with the melting point and viscosity in the range of 1150−1280 °C and 0.2−0.5 Pa·s respectively are suggested. By adopting the suggested slag composition, the industrial tests achieve very high recovery rates of Zn and Pb (97.3% for Zn and 94.5% for Pb), corresponding to slags with a very low average content of Zn and Pb (0.51 wt.% Zn and 0.45 wt.% Pb).

(3) The detoxification of the ZLRs is simultaneously realized after processing in the rotary kiln. After pyrometallurgy in the rotary kiln, the slag is discharged through a wet deslagging system. The National-Standard leaching tests of the water-quenched slags result in 1.82 mg/L Zn, ~0.01 mg/L Cu, 0.0004 mg/L As, ~0.01 mg/L Cd, 0.08 mg/L Pb, and ~0.02 mg/L Hg in the leachate, which are much lower than the standard limiting values.

Acknowledgments

The authors acknowledge the funding support from the National Natural Science Foundation of China (Nos. 51804221, 51874101), the National Key R&D Program of China (No. 2019YFF0217102), and the China Postdoctoral Science Foundation (Nos. 2018M642906, 2019T120684).

References

[1] XING Peng, MA Bao-zhong, ZENG Peng, WANG Cheng-yan, WANG Ling, ZHANG Yong-lu. CHEN Yong-qiang, WANG Shuo, WANG Qiu-yin. Deep cleaning of a metallurgical zinc leaching residue and recovery of valuable metals [J]. International Journal of Minerals, Metallurgy, and Materials, 2017, 24: 1217−1227.

[2] JIA Li-pan, HUANG Jiang-jiang, MA Ze-long, LIU Xu-heng, CHEN Xing-yu, LI Jiang-tao, HE Li-hua, ZHAO Zhong-wei. Research and development trends of hydrometallurgy: An overview based on hydrometallurgy literature from 1975 to 2019 [J]. Transactions of Nonferrous Metals Society of China, 2020, 30(11): 3147−3160.

[3] TURAN M D, ALTUNDOĞAN H S, TŰMEN F. Recovery of zinc and lead from zinc plant residue [J]. Hydrometallurgy, 2004, 75: 169−176.

[4] WANG Le, MU Wen-ning, SHEN Hong-tao, LIU Shao-ming, ZHAI Yu-chun. Leaching of lead from zinc leach residue in acidic calcium chloride aqueous solution [J]. International Journal of Minerals, Metallurgy, and Materials, 2015, 22: 460−466.

[5] MOTAMEDIZADEH M, AZIZI A, BAHRI Z. Recycling lead from a zinc plant residue (ZPR) using brine leaching and cementation with aluminum powder [J]. Environmental Science and Pollution Research International, 2021, 28: 42121−42134.

[6] ZHU Xiao-lin, XU Cun-ying, TANG Jie, HUA Yi-xin, ZHANG Qi-bo, LIU Hai, WANG Xiang, HUANG Meng-ting. Selective recovery of zinc from zinc oxide dust using choline chloride based deep eutectic solvents [J]. Transactions of Nonferrous Metals Society of China, 2019, 29(10): 2222−2228.

[7] ZHANG Chun, MIN Xiao-bo, CHAI Li-yuan, ZHANG Jian-qiang, WANG Mi. Mechanical activation-assisted reductive leaching of cadmium from zinc neutral leaching residue using sulfur dioxide [J]. JOM, 2015, 67: 3010−3021.

[8] RAO Shuai, LIU Zhi-qiang, WANG Dong-xin, CAO Hong-yang, ZHU Wei, ZHANG Kui-fang, TAO Jin-zhang. Hydrometallurgical process for recovery of Zn, Pb, Ga and Ge from Zn refinery residues [J]. Transactions of Nonferrous Metals Society of China, 2021, 31(2): 555−564.

[9] LI Mi, PENG Bing, CHAI Li-yuan, PENG Ning, XIE Xian-de, YAN Huan. Technological mineralogy and environmental activity of zinc leaching residue from zinc hydrometallurgical process [J]. Transactions of Nonferrous Metals Society of China, 2013, 23(5): 1480−1488.

[10] XIE Feng, CHEN Jun-nan, WANG Jian, WANG Wei. Review of gold leaching in thiosulfate -based solutions [J]. Transactions of Nonferrous Metals Society of China, 2021, 31(11): 3506−3529.

[11] KURSUNOGLU S, TOP S, KAYA M. Recovery of zinc and lead from Yahyali non-sulphide flotation tailing by sequential acidic and sodium hydroxide leaching in the presence of potassium sodium tartrate [J]. Transactions of Nonferrous Metals Society of China, 2020, 30(12): 3367−3378.

[12] TURAN M D. Characterization and leaching of mechanically activated zinc residue [J]. Chemical Papers, 2021, 75: 2881−2890.

[13] WANG Hong-jun, FENG Ya-li, LI Hao-ran, KANG Jin-xing. Simultaneous extraction of gold and zinc from refractory carbonaceous gold ore by chlorination roasting process [J]. Transactions of Nonferrous Metals Society of China, 2020, 30(4): 1111−1123.

[14] CAO Lei, LIAO Ya-long, SHI Gong-chu, ZHANG Yu, GUO Mu-yuan. Leaching behavior of zinc and copper from zinc refinery residue and filtration performance of pulp under the hydrothermal process [J]. International Journal of Minerals, Metallurgy, and Materials, 2019, 26: 21−32.

[15] SHEN Xiao-yi, LIANG Yuan-yong, SHAO Hong-mei, SUN Yi, LIU Yan, ZHAI Yu-chun. Extraction and kinetic analysis of Pb and Sr from the leaching residue of zinc oxide ore [J]. International Journal of Minerals, Metallurgy, and Materials, 2021, 28: 201−209.

[16] GARGUL K, BORYCZKO B, BUKOWSKA A, JAROSZ P, MAŁECKI S. Leaching of lead and copper from flash smelting slag by citric acid [J]. Archives of Civil and Mechanical Engineering, 2019, 19: 648−656.

[17] WANG Jie, ZHANG Ying-yi, CUI Kun-kun, FU Tao, GAO Jian-jun, HUSSAIN S, ALGARNI T S. Pyrometallurgical recovery of zinc and valuable metals from electric arc furnace dust—A review [J]. Journal of Cleaner Production, 2021, 298: 126788.

[18] STEWART D J C, BARRON A R. Pyrometallurgical removal of zinc from basic oxygen steelmaking dust—A review of best available technology [J]. Resources, Conservation and Recycling, 2020, 157: 104746.

[19] LIN Xiao-long, PENG Zhi-wei, YAN Jia-xing, LI Zhi-zhong, HWANG J Y, ZHANG Yuan-bo, LI Guang-hui, JIANG Tao. Pyrometallurgical recycling of electric arc furnace dust [J]. Journal of Cleaner Production, 2017, 149: 1079−1100.

[20] LIANG Zhi-kai, YI Ling-yun, HUANG Zhu-chun, LU Biao, JIANG Xiong, CAI Wei, TIAN Bai-zhou, JIN Yun-yun. Insight of iron ore−coal composite reduction in a pilot scale rotary kiln: A post-mortem study [J]. Powder Technology, 2019, 356: 691−701.

[21] YI Ling-yun, ZHANG Nan, LIANG Zhi-kai, WANG Ling, XIAO Hua-rong, HUANG Zhu-cheng. Coal ash induced ring formation in a pilot scale rotary kiln for low-grade iron ore direct reduction process: Characterization and mechanism [J]. Fuel, 2022, 310: 122342.

[22] JI F Z, SICHEN D, SEETHARAMAN S. Experimental studies of the viscosities in the CaO−Fe_nO−SiO_2 Slags [J]. Metallurgical and Materials Transactions B, 1997, 28: 827−834.

[23] CHEN M, ZHAO B J. Viscosity measurements of SiO_2−FeO−CaO system in equilibrium with metallic Fe [J]. Metallurgical and Materials Transactions B, 2015, 46: 577−584.

[24] ZHANG Jun, QI Yuan-hong, YAN Ding-liu, CHENG Xiang-li, HE Peng. Characteristics and mechanism of reduction and smelting-separation process of copper slag [J]. Journal of Iron and Steel Research, International, 2015, 22(2): 121−127.

[25] KLEMETTINEN L, AVARMAA K, TASKINEN P. Slag chemistry of high-alumina iron silicate slags at 1300 °C in WEEE smelting [J]. Journal of Sustainable Metallurgy, 2017, 3: 772−781.

[26] GUO Zheng-qi, ZHU De-qing, PAN Jian, YAO Wei-jie, XU Wu-qi, CHEN Ji-nan. Effect of Na_2CO_3 addition on carbothermic reduction of copper smelting slag to prepare crude Fe−Cu alloy [J]. JOM, 2017, 69: 1688−1695.

[27] ABDEYAZDAN H, FALLAH-MEHRJARDI A, HIDAYAT T, SHEVCHENKO M, HAYES P C, JAK E. The effect of MgO on gas−slag−matte−tridymite equilibria in fayalite-based copper smelting slags at 1473 K (1200 °C) and 1573 K (1300 °C), and $P(SO_2)$=0.25 atm [J]. Journal of Phase Equilibria and Diffusion, 2020, 41: 44−55.

[28] GUO Zheng-qi, PAN Jian, ZHU De-qing, ZHANG Feng.

Co-reduction of copper smelting slag and nickel laterite to prepare Fe−Ni−Cu alloy for weathering steel [J]. JOM, 2018, 70: 150−154.

[29] ZHANG Hai-pei, LI Bo, WEI Yong-gang, WANG Hua, YANG Yin-dong, MCLEAN A. Reduction of magnetite from copper smelting slag in the presence of a graphite rod [J]. Metallurgical and Materials Transactions B, 2020, 51: 2663−2672.

回转窑内渣成分优化实现锌铅元素的高效回收

林泓富[1,2]，翁 威[2,3]，衷水平[2,3]，邱冠周[1]

1. 中南大学 资源加工与生物工程学院，长沙 410083；
2. 紫金矿业集团 低品位难处理黄金资源综合利用国家重点实验室，上杭 364200；
3. 福州大学 紫金地质与矿业学院，福州 350108

摘 要：在回转窑内从高硅锌浸出渣中实现高效回收锌铅金属。XRD、SEM、EDS 及 ICP 表征结果表明，浸出渣含 12.4% SiO_2、16.1% Zn 和 7.4% Pb(质量分数)。热力学分析表明，在回转窑内 1150~1250 ℃的冶炼环境下，锌浸出渣中极易产生锌和铅的金属蒸气。通过分析 13 种冶金渣成分的黏度及熔点，发现 3 种渣成分(47%SiO_2−23%CaO−30%FeO、40%SiO_2−28%CaO−32%FeO、40%SiO_2−30%CaO−30%FeO，质量分数)具有合适的物理特性，即熔点和黏度分别为 1150~1280 ℃和 0.2~0.5 Pa·s。工业实验表明，采用优化的渣成分，锌和铅的回收率分别高达 97.3%和 94.5%, 冶炼后渣内锌和铅的含量分别低至 0.51%和 0.45%(质量分数)。水淬渣的国标浸出实验表明，浸出液中含 1.82 mg/L Zn、~0.01 mg/L Cu、0.0004 mg/L As、~0.01 mg/L Cd、0.08 mg/L Pb 和~0.02 mg/L Hg，证实锌浸出渣同步实现无害化。

关键词：锌浸出渣；金属回收；回转窑；渣型调控；无害化处置

(Edited by Xiang-qun LI)